Flows Created by a Cylinder with Oscillatory Translation and Spin

Hugh M. Blackburn[1,2], John R. Elston[2] and John Sheridan[2]
[1]*CSIRO Building, Construction and Engineering*
PO Box 56 Highett Vic 3190, AUSTRALIA
hmb@dbce.csiro.au
[2]*Department of Mechanical Engineering*
Monash University, Clayton 3168, AUSTRALIA

1 Abstract

Our work initiates the study of flows resulting from the combination of oscillatory translation and rotation of a circular cylinder. A direct numerical simulation approach has been employed in which a spectral element spatial discretization was used to solve the two-dimensional incompressible Navier–Stokes equations in an accelerating reference frame attached to the cylinder. Cylinder spin was imposed by use of time-varying velocity boundary conditions at the cylinder wall. The simulation results to be presented were conducted with a Reynolds number of 200, based on the cylinder diameter and the RMS translational velocity, and with a constant Keulegan–Carpenter number of π, corresponding to a peak-to-peak translation amplitude of one cylinder diameter. In addition, the spin amplitude was set so that the peak cylinder tangential velocity matched the peak translational velocity. Even with these restrictions, a wide variety of flows was observed as the phase angle between cylinder translational and spin oscillations was changed.

2 Introduction

Flow separation produced by oscillatory flow normal to the axis of a cylindrical bluff body (Williamson 1985) or equivalently the oscillatory translation of the bluff body in quiescent fluid is known to result in a variety of different vortex shedding modes, dependent on the Reynolds and Keulegan–Carpenter (KC) numbers. For steady flow past a circular cylinder, it has also been shown that the imposition of an oscillatory rotational motion about the cylinder axis is able to bring about substantial changes to the wake (Tokumaru & Dimotakis 1991), again depending on the Reynolds number, the rotational equivalent of the KC number and additionally the Strouhal number of the oscillation. The work of Tokumaru & Dimotakis suggests that control exerted on the wake by the rotational oscillation is greatest when the frequency of oscillation is approximately the same as the Strouhal frequency for the unforced wake. No published investigation has yet addressed the combined effects of oscillatory translation and rotation.

On the other hand it is known that the propulsion mechanism used by fish and some other animals depends on a flapping motion combined with a phase-locked twisting (*carangiform motion*, see Ch. 11, Lighthill 1986). The resulting flow forms a wake which moves normal to the flap direction and, correspondingly, pressure forces are exerted on the flapping fin which provide the animal with thrust. It occurred to us that the important feature of the fin's motion is the control of vorticity creation and release by the Kutta condition at the trailing edge and that an analogous control over the vorticity shed by a cylinder in translational oscillation might be exerted by imparting an oscillatory spin to the cylinder.

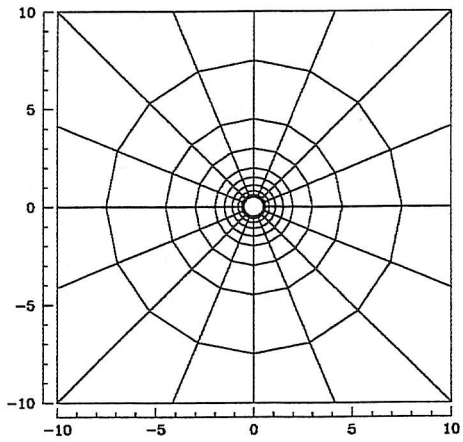

Figure 1: Spectral element mesh used for calculations.

p	4	6	8	10
$\widehat{C}_l$	7.630	7.622	7.620	7.620

Table 1: p-Convergence results for the translating cylinder, where p is the order of tensor-product GLL Lagrange interpolant shape function employed in each spectral element.

We have carried out an exploratory investigation of combined oscillatory translation and rotation of a circular cylinder using two-dimensional numerical simulations. Assuming simple harmonic motions for both translation and rotation, the problem has five dimensionless parameters: the KC number, a Reynolds number, the ratio of translation and rotation frequencies, the ratio of peak cylinder translational and tangential velocities, and the phase angle between the simple harmonic motions of translation and rotation. For simplicity we have chosen the amplitude of translational motion to be $0.5\,D$, $KC = 2\pi A/D = \pi$; the translational and rotational frequencies to be the same; the peak translational and tangential velocities to be the same; the Reynolds number fixed; $Re = \sqrt{2}\pi AfD/\nu = 200$, where A is the amplitude of translational motion, f its frequency and D the cylinder diameter. The only varied parameter was the phase angle between the two motions (ϕ).

3 Method

Simulations were carried out using a spectral element spatial discretization to solve the two-dimensional incompressible Navier–Stokes equations in an accelerating reference frame attached to the cylinder, as previously described in Blackburn & Henderson (1996). Cylinder spin was imposed by use of time-varying boundary conditions at the cylinder wall. For all the results described here, solutions were obtained in a square domain of size $20D \times 20D$, with the 144-element mesh shown in figure 1.

In order to ease requirements on mesh size, periodic boundaries were used on the mesh exterior, so the simulations can also be taken to represent those for a periodic array of circular cylinders, each with translation and spin. Convergence results for the peak coefficient of lift are presented in table 1 (C_l was computed using the cylinder's RMS velocity and diameter).

These show that the results were effectively converged with 8th-order tensor-product Gauss–Legendre–Lobatto (GLL) shape functions. However, 10th order shape functions have been used for the computation of all the results to be presented.

4 Vorticity production

The contour plots which follow are of the single non-zero vorticity component: this was computed in post-processing from the primitive variable simulation results via collocation differentiation. The contours are shown in a fixed reference frame. For a two-dimensional flow of Newtonian incompressible fluid the equation for the vorticity source strength at solid walls in an inertial reference frame reads (Morton 1984)

$$-\nu\, \boldsymbol{n} \cdot \boldsymbol{\nabla\omega} = -\boldsymbol{n} \times (\boldsymbol{\nabla} P + \boldsymbol{a}), \tag{1}$$

where $\boldsymbol{\omega}$ is the vorticity vector, $P = p/\rho$ is the kinematic pressure, $\boldsymbol{n}$ is a unit wall-normal vector, $\boldsymbol{a}$ is the wall acceleration and all terms are evaluated at the wall. This equation expresses the idea that vorticity must diffuse away from a solid boundary at the same rate that it is produced by local conditions. When the cylinder motion consists only of translational oscillation, the integral of the vorticity flux around the periphery of the cylinder must be zero at every instant. When the cylinder has also an oscillatory rotation at the same frequency as the translation, the net vorticity flux integrated over one motion cycle is zero, but the instantaneous requirement must be relaxed.

5 Translational oscillation

Figure 2 shows vorticity contours for the case where the cylinder executes only translational oscillation (in the vertical direction, as for all the simulations), after sufficient simulation time had elapsed for the results to reach a periodic condition. The cylinder is shown in its uppermost position ($y/D = 0.5$), as indicated by the cross-hairs in the figure, which are located at the centre of the cylinder in its rest position. Contours of positive (anticlockwise) vorticity are shown in black, negative vorticity in grey. The vorticity contours are drawn only to an arbitrary maximum magnitude, so that the regions of highest magnitude vorticity are not marked. Figure 2 *a* shows a global view of the whole computational domain while 2 *b* shows a $2D \times 2D$ subset.

In figure 2 *b* there are two detached 'starting' vortices below the cylinder, with unmarked cores in the shape of eyes. These vortices were produced during the upwards motion which has just completed, and at the time shown the vortices are surrounded by closed streamline loops. Immediately adjacent to the surface of the cylinder are thin layers of negative vorticity (on the left side) and positive vorticity (on the right). At the instant shown the cylinder has its maximum downward acceleration and the vorticity at the cylinder surface has resulted largely from the time-integrated effect of acceleration term, $\boldsymbol{n} \times \boldsymbol{a}$ in (1), although the top/bottom asymmetry shows also the influence of the pressure gradient term.

6 Combined translational and rotational oscillation

In order to obtain the results in this section, the cylinder was provided with oscillatory motion in addition to translation. The cylinder translation is described by $y(t) = A_t \cos(2\pi f t)$, while

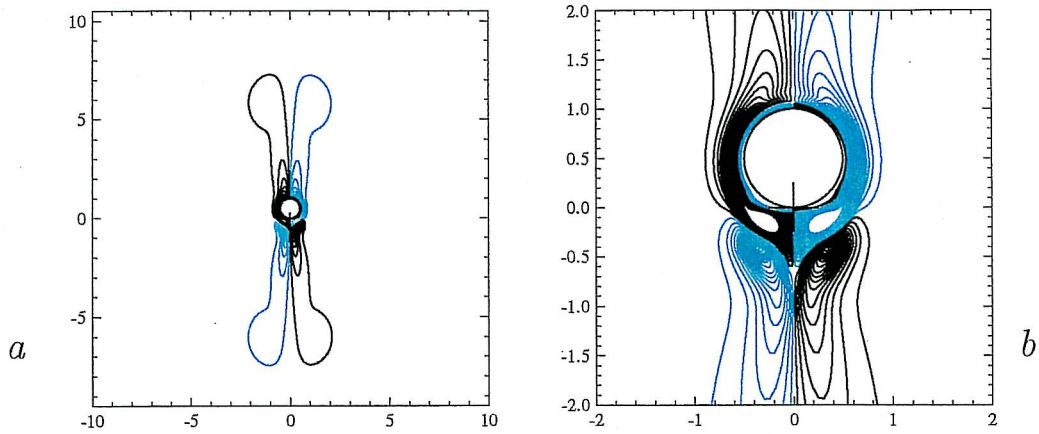

Figure 2: Vorticity contours for the cylinder in oscillatory translation (no spin), at the time when the cylinder is at its highest point in the motion cycle. *a*; global view, *b*; close up.

the rotation is given by $\theta(t) = A_\theta \cos(2\pi ft + \phi)$, with positive angles taken in the anticlockwise sense. Figure 3 displays contours of vorticity at an elapsed dimensionless time $tf = 45.75$ for eight values of phase angle ϕ starting at 0°, increasing in increments of 22.5°. Owing to the physical symmetry of the problem, phase angles greater than 180° give rise to flow patterns that are 180° rotations of those in the range 0–180°.

The variation of phase angle produces a wide variety of different flow configurations. For $\phi = 45°$, 67.5° and 90° it can be seen that vortex pairs have left the computational domain, but re-entered on the opposite side as a result of the periodic domain boundaries. Perhaps the two most intriguing results are the jet flow that arises when $\phi = 0°$ and the double-jet 'butterfly' flow for $\phi = 157.5°$.

The jet flow produced when $\phi = 0°$ is normal to the axis of cylinder translation and thus it corresponds to the propulsive jet produced by carangiform motion, and in fact the phase relationship between translation and rotation in this case is the same as for carangiform motion. The production of the jet is consistent with the fact that a time-mean force is exerted on the cylinder in the negative-x direction: $\overline{C}_d = -0.159$, where the velocity used in calculating C_d is the RMS cylinder velocity.

Figure 4 shows a close-up view of vorticity contours at four instants in half a cycle of cylinder motion, starting at the uppermost position, which also has the greatest angular displacement, as indicated by the radial line on the cylinder. It is notable that the most active area of vorticity production appears to be the left surface of the cylinder, which is to be expected from the surface-tangential acceleration production term $\boldsymbol{n} \times \boldsymbol{a}$ in (1), since this is always larger in magnitude on the left side of the cylinder for the case $\phi = 0°$. It is interesting that this subsequently leads to a vorticity transport to the right of the cylinder, an effect which is apparently due to interaction between the sequence of different shear layers that are produced as the cylinder spins and translates.

7 Conclusions

It has been shown that the combination of oscillatory translation and rotation of a circular cylinder is able to produce a variety of flows, here controlled by the phase angle between the

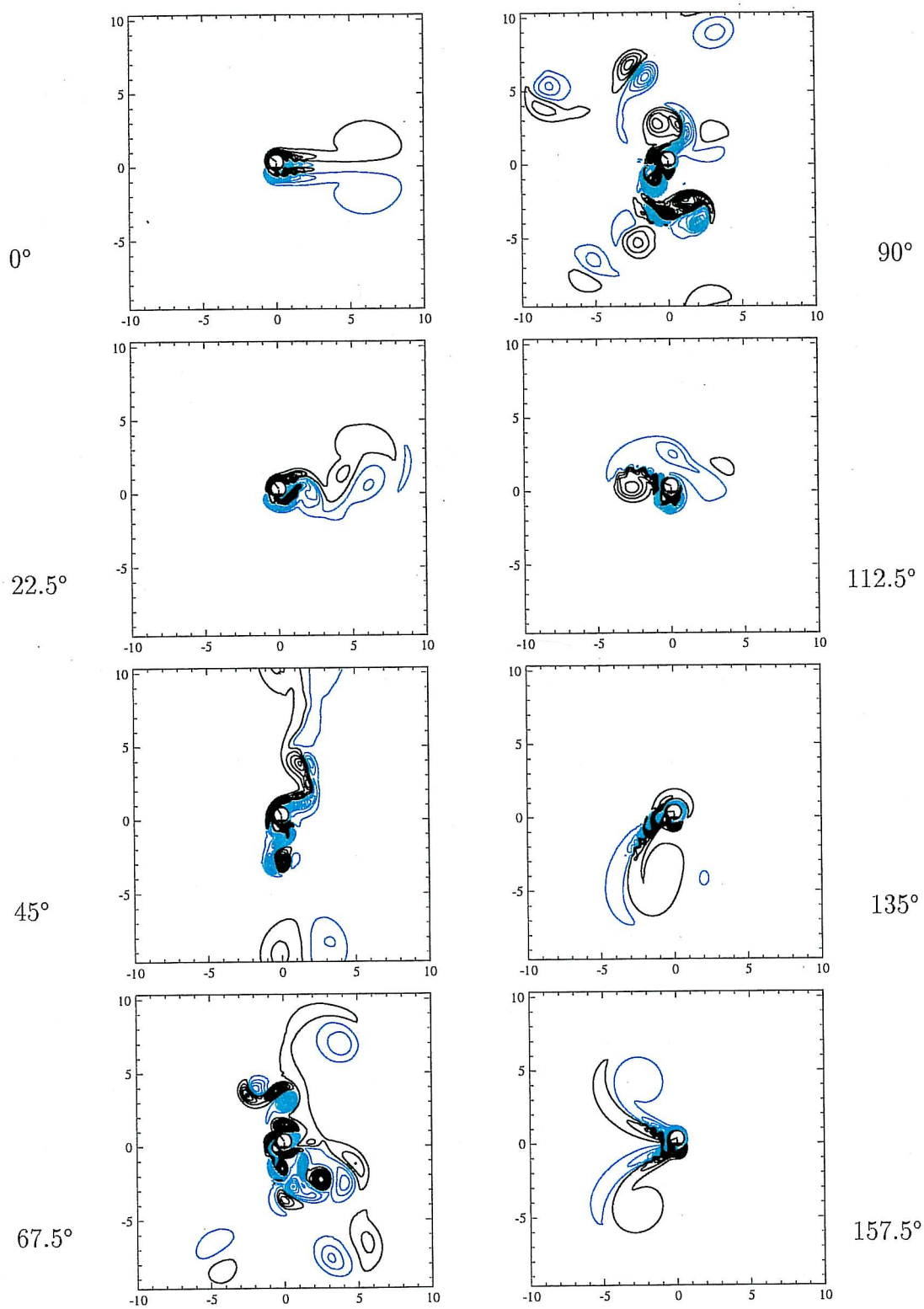

Figure 3: Vorticity contours at elapsed time $tf = 45.75$ for different phase angles ϕ.

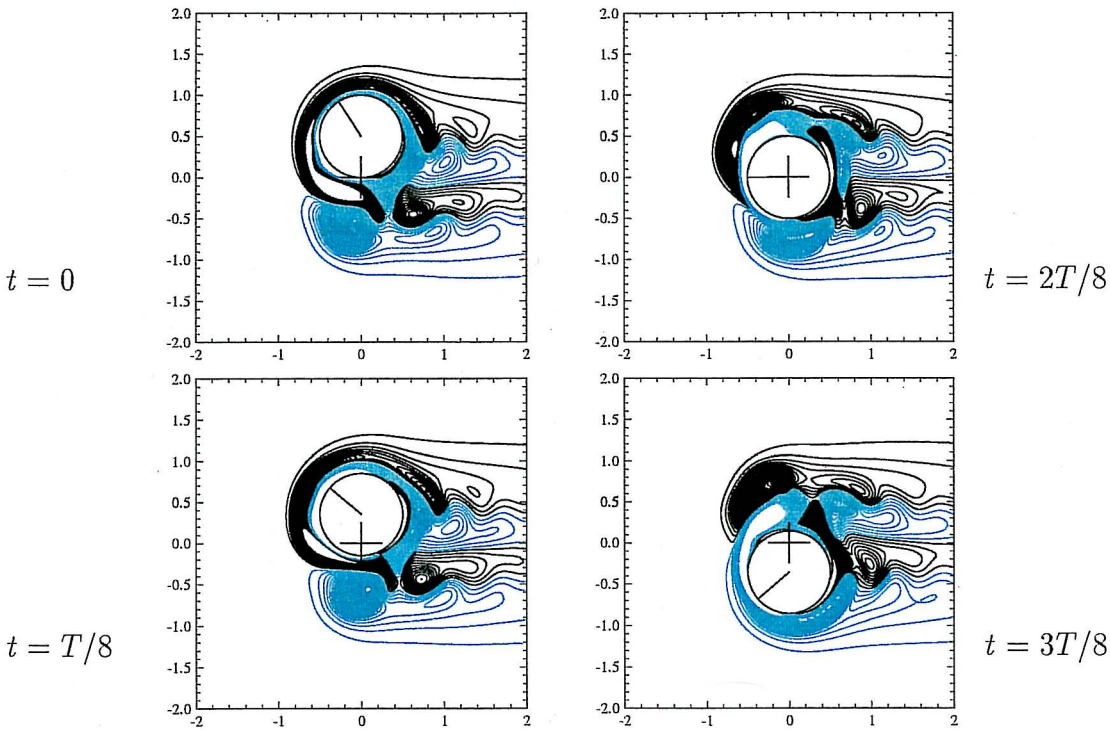

Figure 4: Vorticity contours for the cylinder in oscillatory translation and rotation for the case $\phi = 0°$. Four detail views illustrating half a motion cycle, period T.

translation and spin motions. For the case where the phase angle is zero, a jet of fluid is produced in the direction normal to the translation axis, leading to a time-mean thrust on the cylinder. The apparent analogy to the thrusting mechanism employed by fast-swimming fish has been noted but remains to be explored in more detail.

References

Blackburn, H. M. & Henderson, R. D. (1996). Lock-in behaviour in simulated vortex-induced vibration, *Exptl Thermal & Fluid Sci.* **12**(2): 184–189.

Lighthill, J. (1986). *An Informal Introduction to Theoretical Fluid Mechanics*, Oxford University Press.

Morton, B. R. (1984). The generation and decay of vorticity, *Geophys. Astrophys. Fluid Dyn.* **28**: 277–308.

Tokumaru, P. T. & Dimotakis, P. E. (1991). Rotary oscillation control of a cylinder wake, *J. Fluid Mech.* **224**: 77–90.

Williamson, C. H. K. (1985). Sinusoidal flow relative to circular cylinders, *J. Fluid Mech.* **155**: 141–174.